

Broadband negative acoustic radiation force by a soft thin plate patterned with periodical heavy grating

Hailong He, Shiliang Ouyang, Zhaojian He^{a)}, Ke Deng^{a)}, and Heping Zhao

Department of Physics, Jishou University, Jishou 416000, Hunan, China

Abstract

We investigate the acoustic radiation force (ARF) acting on a cylindrical brass particle near a soft thin plate patterned with periodical heavy grating. The existence of negative ARF is confirmed by which the particle near the surface of plate can be pulled backward. In addition, bandwidth for negative ARF in this soft plate system is found to be considerably broader compared with the stiff plate systems usually used in existing works. It is further demonstrated by field distribution analysis that this interesting negative ARF stems from the collective resonant excitation of the antisymmetric intrinsic Stoneley surface waves in the thin plate. Properties of ARF varying with the particle location and particle size are also investigated. The reported negative ARFs will have extensive application in manipulating particles by using of acoustic wave.

I. INTRODUCTION

Acoustic waves can produce acoustic radiation forces (ARFs) when illuminating on objects as the result of momentum exchange between the objects and incident field [1, 2]. In most situations, such forces are positive as acoustic waves usually push objects towards the propagating direction. However, it is the counterintuitive negative ARF (acoustic waves pulling the objects continuously towards the wave source direction) that is much more desirable, since the pulling effect is a key function for a wide range of acoustic applications such as particle manipulations [3-7] and acoustic levitations [8]. It has been proved that negative ARFs can be obtained by utilizing nondiffracting

^{a)}Authors to whom correspondence should be addressed: hezj@jsu.edu.cn and dengke@jsu.edu.cn.

acoustic beams such as the Bessel beams [9-14] or crossed plane waves [15, 16]. In these cases, asymmetry of the scattered field (forescattering dominates the backscattering) plays the crucial role for the emergence of these pulling effects. More complicated manipulations including sharp bending of microparticles by acoustic half-Bessel beams has also been successfully demonstrated very recently [17].

In the past few years, acoustic artificial structured plates have attracted much interest owing to their exotic intrinsic modes [18-20]. In particular, resonant excitation of the antisymmetric Lamb waves in an acoustically stiff plate can lead to extraordinary enhanced acoustic transmissions [21]. Unique vortex near-field patterns were confirmed in such exotic wave responses, which provide a rich diversity for the interactions between waves and objects. Acoustic trapping of small particles immersed in such vortex near-fields of a periodically structured brass plate immersed in water have been reported in previous works [3, 4]. It was also further demonstrated that ARFs exerting on rigid wall can be remarkably amplified through the aid of the resonant coupling with adjunctive metamaterial slabs [22]. Moreover, a recent work investigated interactions between a pair of stiff structured plates in which the near-field coupling caused attracting force were reported [23].

In this paper, acoustic radiation forces acting on a cylindrical brass particle by an acoustically soft plate patterned with periodical heavy grating are investigated. It is confirmed that the ARF could turn negative when the particle is immersed in the vortex near-fields of the plate. In addition, bandwidth for negative ARF in this soft plate system is found to be considerably broader compared with the previous stiff plate systems [3, 4], with a full width at half maximum (FWHM) in negative ARF spectra being four times larger than that of Ref. 3. It is further demonstrated by field distribution analysis that this negative ARF stems from the gradient force induced by the gradient vortex velocity field near the surface. Properties of ARF varying with the particle location and particle size are also investigated. Prospective applications of such broadband negative ARFs could be predicted.

II. THEORY AND RESULTS

TABLE I . Material parameters.

	Density [kg/m ³]	Longitude velocity[m/s]	Transverse velocity[m/s]
Water	1000	1490	
Epoxy	1800	2740	1600
Brass	8600	4400	2100

To be specific, the system under study is a water-immersed epoxy plate (marked with yellow rectangle) of thickness t , patterned with periodical brass grating (marked with black squares) on the bottom, as shown in Fig. 1(a). The period for the grating is the lattice constant d , and the side length of the brass strip is a . A cylindrical brass particle (marked with black circle) of radii R is placed above the plate with a separation distance Δy [shown in the inset of Fig. 1(a)] from the bottom of particle to the plate, and a distance Δx from the particle's center to the central axis perpendicular to the plate [corresponding to the Y axis in Fig. 1(a)]. The material parameters under study are listed in Table I. Throughout the paper, the finite element method based on COMSOL Multiphysics software is employed to conduct numerical simulations, in which perfectly matched layers (PMLs) are used at the computational boundaries to prevent reflections. The overall size of the simulation domain is approximately $50d \times 10d$, corresponding to 50 grating periods. Unless otherwise specified, we set $R=0.2d$, $t=0.245d$, $a=0.21d$, $\Delta x=0.0d$ and $\Delta y=0.05d$, respectively. The frequency is normalized by c_0/d , where c_0 is the speed of acoustic wave in water.

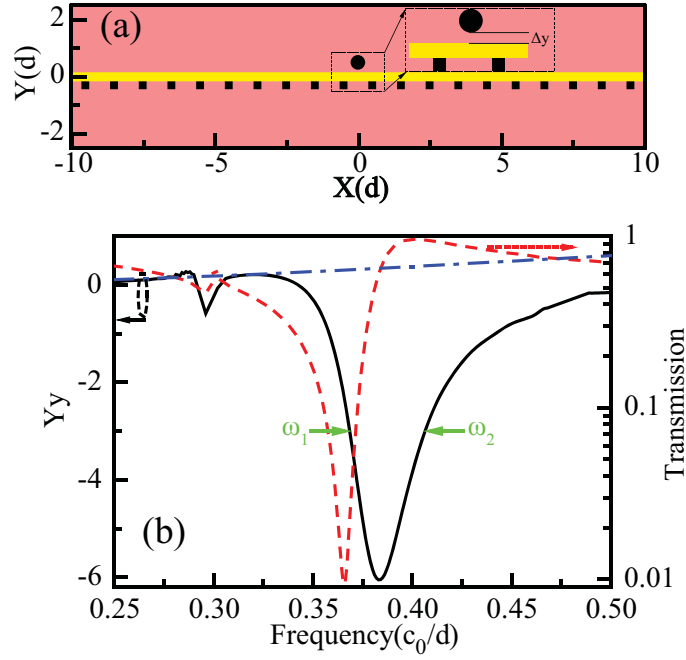


FIG. 1. (Color online) (a) Schematic view of the soft plate patterned with periodical brass grating on the bottom of plate. A cylindrical brass particle is placed above the structured plate. (b) The transmission (in \log_{10} scale, marked with red dashed line) and dimensionless ARF function Y_y exerted on the brass particle (marked with black solid line) for the system under Gaussian beam (of width $\sim 10d$) normal incidence from the bottom. For comparison, the dimensionless ARF function Y_y exerted on the brass particle without plate is also shown with blue dot-dash line.

The ARF acting on a cylindrical particle can be represented by [9, 15, 17, 22-25]

$$\mathbf{F} = -\oint \langle \mathbf{S} \rangle \cdot d\mathbf{A}, \quad (1)$$

where the differential area $d\mathbf{A} = \mathbf{n}dA$, \mathbf{n} is the normal directed away from the particle, A is the particle's surface at its equilibrium position, and $\langle \mathbf{S} \rangle$ is the time-averaged momentum-flux tensor, which is given by

$$\langle \mathbf{S} \rangle = \frac{\langle p^2 \rangle}{2\rho_0 c_0^2} \mathbf{I} - \frac{\rho_0 \langle |\mathbf{V}|^2 \rangle}{2} \mathbf{I} + \rho_0 \langle \text{Re}(\mathbf{V}^* \mathbf{V}) \rangle. \quad (2)$$

Here \mathbf{V} and p are the first-order velocity and pressure fields respectively, \mathbf{I} is a unit tensor, ρ_0 and c_0 are the mass density and sound speed of the surrounding water.

The dimensionless ARF function $Y_{x(y)} = F_{x(y)}/I_0$ is used to evaluate the force on the

particle, where I_0 is defined as the incident acoustic wave energy density across the particle position in the absence of particle [3, 23, 24,].

In Fig. 1(b), we exhibit the transmission spectra (red dashed line) and dimensionless ARF Y_y (black solid line) of the system with a Gaussian beam normally incident from bottom of the plate. Here, the width of the Gaussian beam is $10d$. For normal incidence, Y_x becomes zero because of the symmetry of the system with respect to the Y-axis, and thus is not displayed here. It can be seen from Fig. 1(b) that there exists an abnormal transmission dip at frequency $0.368(c_0/d)$, which is resulted from the resonant excitation of the antisymmetric Stoneley waves in the plate [26-28]. Under the excitation of these antisymmetric modes, a collective resonance of the thin plate is induced and further gives rise to a negative dynamic mass [27]. In addition, it is observed that the dimensionless ARF Y_y becomes negative in a considerable frequency range around the transmission dip, which indicates that the brass particle is in face undergoing pulling force for these frequencies. Here we notice that similar negative ARFs were also observed for periodically structured brass plates, in which the negative ARF spectra lies around the resonant transmission peak of the stiff plate systems [3, 4]. To give some quantitative comparisons for the bandwidth of pulling force in these two systems, we calculate the FWHMs of the negative ARF spectra, both for the soft plate system considered here and the stiff brass plate system in Ref. 3. The relative FWHM of negative force for our soft plate system is

$$\Delta = \frac{2(\omega_2 - \omega_1)}{\omega_1 + \omega_2} = 9.7\% \quad [\text{here } \omega_1 \text{ and } \omega_2 \text{ are marked by green arrows in Fig. 1(b)},]$$

which is found to be considerably larger than (about four times of) that of the brass-plate system ($\Delta = 2.4\%$). Moreover, for comparison, the dimensionless acoustic force exerted on a brass particle immersed in a pure Gaussian beam without the plate is also shown by blue dot-dash line in Fig. 1(b), which exhibits uniform positive forces as expected.

III. DISCUSSIONS

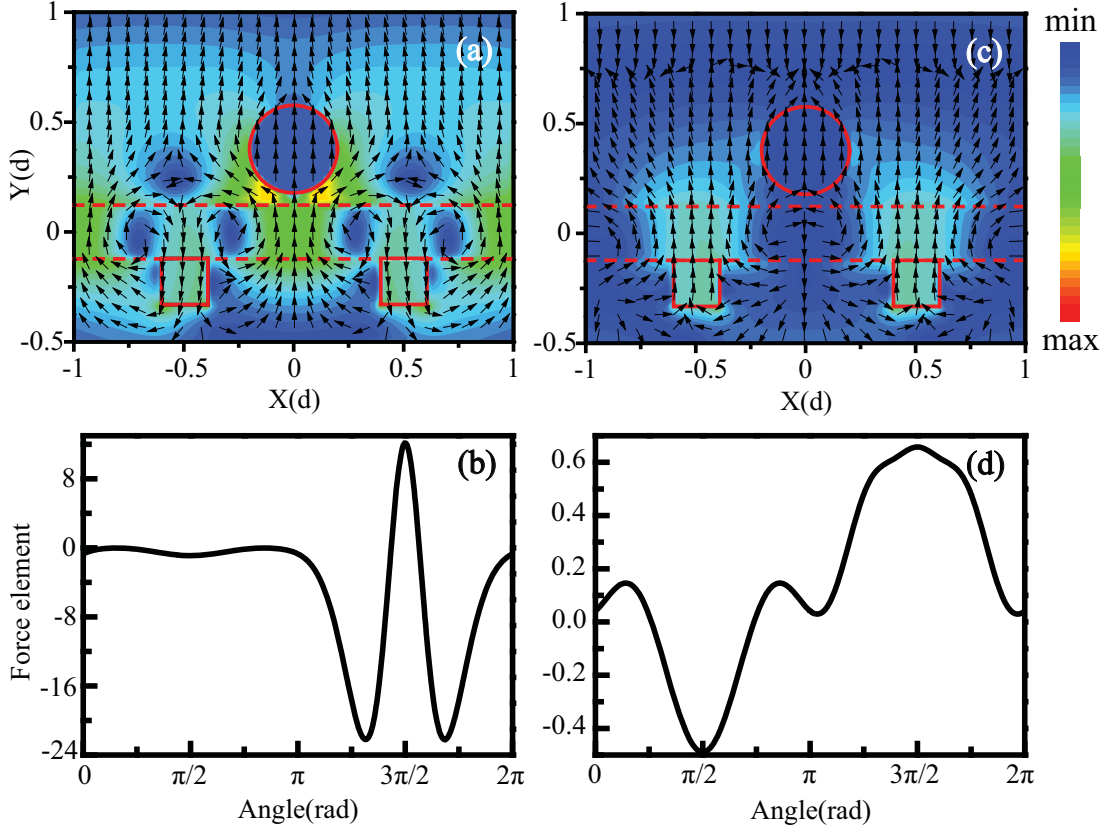


FIG. 2 (Color online) The velocity field distributions and y-direction force elements of our system for the resonant frequency $0.383(c_0/d)$ [(a) and (b)] and for a non-resonant frequency $0.32(c_0/d)$ [(c) and (d)].

In order to further elucidate how the negative ARF incurs under the resonant excitation of antisymmetric Stoneley waves, we investigate the velocity field distributions and y-direction force elements across the particle, for both the negative and positive ARF frequencies. In Fig. 2(a), we exhibit the velocity field distribution at the frequency $0.383(c_0/d)$ for which the maximum negative ARF is observed. It can be seen that vortex and anti-vortex field patterns are reproduced due to the excitation of antisymmetric Stoneley waves in the system as analyzed in Ref. 27. We also calculate the y-direction force elements across the particle at $0.383(c_0/d)$ and show the result in Fig. 2(b). The dimensionless ARF Y_y on the whole particle can be obtained by integrating these force elements [3]. Here the angle in Fig. 2(b) represents the action spot of the force element which is measured according to the X axis: The radian 0 means the rightmost part of our integrating circle, and so forth. We can see that the

force elements are almost zero from 0 to π across the particle. However, there exist strong negative force elements from π to $4\pi/3$ and from $5\pi/3$ to 2π across the particle. Although the particle undergoes some strong pushing forces from $4\pi/3$ to $5\pi/3$, after integrating all the force elements across the particle, the total force exerting on the particle is still negative. Through analyzing the corresponding field patterns in Fig. 2 (a), we find that vortex and anti-vortex patterns exist in these regions, which lead to the negative force on the particle. For comparison, we also calculate the field distributions and y-direction force elements across the brass particle at a normal frequency $0.32(c_0/d)$ without resonance, the results are shown in Fig. 2(c) and (d). It can be seen that there is no gradient vortex and anti-vortex patterns field in Fig. 2(c), and the acoustic waves can directly go through the plate to give the particle a pushing effect. Correspondingly, the force elements across the particle are almost near zero value, and the integration of the force elements is positive, incurring a push force as analyzed from the field.

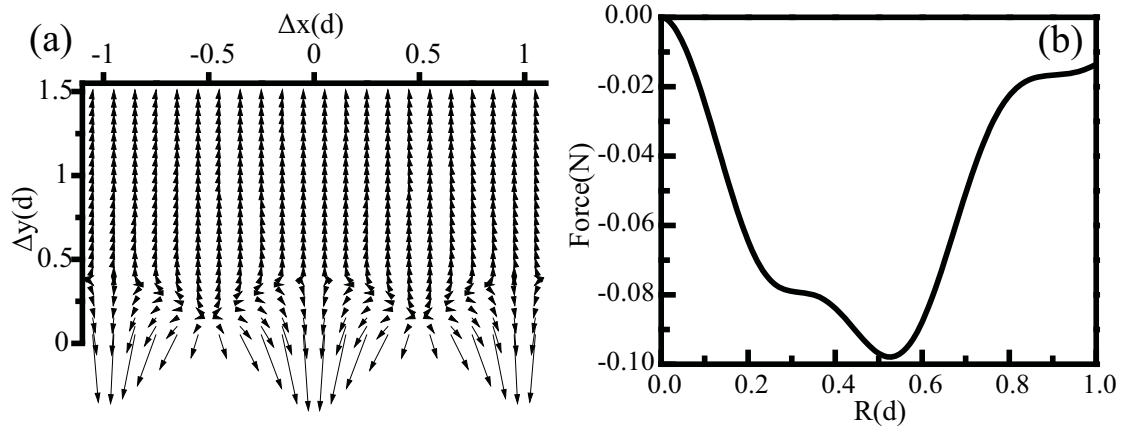


FIG. 3 (a) The radiation force map exerted on the brass particle with position Δx from $-1.05d$ to $1.05d$ and Δy from $0.05d$ to $1.05d$ for the system under resonance. The radii of the particle is $0.2d$. (b) The y-directional net force exerted on the particle with different radius but keeping the separation $\Delta y=0.05d$.

Fig. 3(a) gives the spatial distribution for total ARF of the particle with radii $0.2d$ at

frequency $0.383(c_0/d)$. Here the position for the particle ranges from $-1.05d$ to $1.05d$ for Δx , and from $0.05d$ to $1.5d$ for Δy . The direction and length of the arrows in Fig. 3(a) indicate the ARF direction and intensity, respectively. It can be clearly seen that the particle undergoes pulling forces for Δy smaller than $0.4d$. In addition, the force becomes larger when the particle move more close to the plate. This force distribution is consistent with the properties we obtained from field distribution in Fig. 2. We also investigate the influence of particle radii on the ARF. In Fig. 3(b), we exhibit the y-direction net force of the particle at the position $\Delta x=0.0d$ and $\Delta y=0.05d$ with different radius. It can be observed that there is a dip at radii $R=0.5d$. From the radiation force map in Fig. 3(a), we can conclude that when the effective area of negatively forced surface (area immersed in the near resonant field) becomes larger, the y-direction pulling force will be more negative. Hence, when radii of the particle increases from zero to $0.5d$, the net pulling force increases as shown in Fig. 3(b). However, continuing to increase the radii would make the upper part of the particle be away from the gradient resonant field, and this part would undergo a pushing (positive) force. Although the forcing area of the particle in the near resonant field increases, the interactions of these two competitions causes the pulling effect to be weakened when the radii of the particle further increases from the critical point ($R=0.5d$).

As we have demonstrated in the second section, the negative ARF of our soft-plate-system exhibits a broadband property compared to the stiff plate ones usually used in most previous works [3, 4]. For both the soft and stiff systems, negative ARFs arise from the gradient vortex velocity near-field around the frequency range in which the abnormal transmission (for stiff plates) or reflection (for soft plates) occurs. For the stiff plate, the frequency range of abnormal transmission is usually relatively narrower (and sometimes sharper) compared to that of abnormal reflection in a soft plate. This stems from the difference of material property between stiff and soft plates. For a stiff plate, the intrinsic asymmetric modes are hard to excited and the vortex near-field patterns do not appear unless the frequency of exciting waves is very close to the resonant one, which leads to a narrow transmission spectrum [3, 21]. While for our soft plate patterned with

periodical heavy grating, as a combined result of the weak elastic modulus in plate and the large mass density of the grating, intrinsic modes of this systems can be excited even under the condition that the frequency of external exciting is a bit far away from the resonant one, leading to a relatively broad reflection spectrum. In other words, the vortex near-field patterns can be excited by a broadband acoustic wave impinging on our system [27]. Therefore, our soft-plate system exhibits a broadband property compared to the stiff plate one.

It should be pointed out that the negative ARF dip is not consistent with the transmission dip in Fig. 1(b). As we have demonstrated, the collective resonant excitation of the antisymmetric intrinsic Stoneley surface waves in the plate leads to an abnormally enhanced reflection of the plate. Vortex near-field patterns in velocity field distribution are produced when this resonant excitation happens, which in turn give rise to the emergence of negative ARFs in this paper. Therefore, emergence of such negative ARFs should be accompanied with the enhanced reflection for our soft-plate system. Despite of this, the transmission dip is not guaranteed to be consistent with the ARF dip. In this paper, the computed transmissions, being defined as the energy flux ratio, are proportional to the pressure field p at the far field. While the y -component ARF acting on a cylindrical particle can be further reduced to [23]

$$F_y = \oint -\rho_0 \operatorname{Re}(v_y^* v_x) dA_x + \left(\frac{\rho_0 |v_x|^2}{2} - \frac{|p|^2}{2\rho_0 c_0^2} - \frac{\rho_0 |v_y|^2}{2} \right) dA_y, \quad (3)$$

which indicates that both the first-order velocity (V) and the pressure fields (p) make contributions to the ARF. In addition, the negative ARF of particle is obtained in the near-field of the plate, in which the pressure p might be very different from that in far field. Therefore, at the frequency of transmission dip, the combined contribution of near-field V and p in Eq. (3) usually does not get the utmost effect. This leads to the deviation of the frequency dips between the negative ARF and the transmission spectra, since the former depends on the combined contribution of V and p in the

near-field, whereas the latter is linked to the p at far field.

IV. CONCLUSIONS

In conclusion, we have demonstrated that a broadband and tunable negative ARF can be obtained by the system consisting of an epoxy plate patterned with periodical brass grating. Broadband property of this negative force stems from the collective excitations of the antisymmetric coupled Stoneley waves in the soft plate with heavy gratings. It is further demonstrated that this negative ARF stems from the gradient force induced by the gradient vortex velocity field near the surface. Properties of ARF varying with the particle location and particle size are also investigated in detail. Such negative ARFs may have potential applications, such as to trapping or manipulate particles in a broad band by acoustic waves.

ACKNOWLEDGEMENTS

This work is supported by the National Natural Science Foundation of China (Grant No. 11104113, 11304119, 11464012 and 11264011), and Natural Science Foundation of Hunan province, China (Grant No. 13JJ6059), and Natural Science Foundation of Education Department of Hunan Province, China (Grant No. 13B091, 13A077 and 13C750).

- [1] F. E. Borgnis, Acoustic radiation pressure of plane compressional waves, *Rev. Mod. Phys.* **25**, 653 (1953).
- [2] T. Hasegawa, Y. Hino, A. Annou, H. Noda, M. Kato, and N. Inoue, Acoustic radiation pressure acting on spherical and cylindrical shells, *J. Acoust. Soc. Am.* **93**, 154 (1993).
- [3] F. Y. Cai, Z. J. He, Z. Y. Liu, L. Meng, X. Cheng, and H. R. Zheng, Acoustic trapping of particle by a periodically structured stiff plate, *Appl. Phys. Lett.* **99**, 253505 (2011).
- [4] F. Li, F. Y. Cai, Z. Y. Liu, L. Meng, M. Qian, C. Wang, Q. Cheng, M. L. Qian, X. Liu, J. R. Wu,

-
- J. Y. Li, and H. R. Zheng, Phononic-crystal-based acoustic sieve for tunable manipulations of particles by a highly localized radiation force, *Phys. Rev. Applied* **1**, 051001 (2014).
- [5] C. R. P. Courtney, C. E. M. Demore, H. X. Wu, A. Grinenko, P. D. Wilcox, S. Cochran, and B. W. Drinkwater, Independent trapping and manipulation of microparticles using dexterous acoustic tweezers, *Appl. Phys. Lett.* **104**, 154103 (2014).
- [6] J. D. Adams and H. T. Soh, Tunable acoustophoretic band-pass particle sorter, *Appl. Phys. Lett.* **97**, 064103 (2010).
- [7] J. Whitehill, A. Neild, T. W. Ng, and M. Stokes, Collection of suspended particles in a drop using low frequency vibration, *Appl. Phys. Lett.* **96**, 053501 (2010).
- [8] D. Foresti, N. Bjelobrk, M. Nabavi, and D. Poulikakos, Investigation of a line-focused acoustic levitation for contactless transport of particles, *J. Appl. Phys.* **109**, 093503 (2011).
- [9] P. L. Marston, Axial radiation force of a Bessel beam on a sphere and direction reversal of the force, *J. Acoust. Soc. Am.* **120**, 3518 (2006).
- [10] P. L. Marston, Negative axial radiation forces on solid spheres and shells in a Bessel beam, *J. Acoust. Soc. Am.* **122**, 3162 (2007).
- [11] P. L. Marston, Radiation force of a helicoidal Bessel beam on a sphere, *J. Acoust. Soc. Am.* **125**, 3539 (2009).
- [12] L. K. Zhang and P. L. Marston, Geometrical interpretation of negative radiation forces of acoustical Bessel beams on spheres, *Phys. Rev. E* **84**, 035601 (2011).
- [13] Y. Choe, J. W. Kim, K. K. Shung, and E. S. Kim, Microparticle trapping in an ultrasonic Bessel beam, *Appl. Phys. Lett.* **99**, 233704 (2011).
- [14] D. Baresch, J. L. Thomas, and R. Marchiano, Three-dimensional acoustic radiation force on an arbitrarily located elastic sphere, *J. Acoust. Soc. Am.* **133**, 25 (2012).
- [15] S. J. Xu, C. Y. Qiu, and Z. Y. Liu, Transversally stable acoustic pulling force produced by two crossed plane waves, *Europhys. Lett.* **99**, 44003 (2012).
- [16] C. E. M. Démoré, P. M. Dahl, Z. Y. Yang, P. Glynne-Jones, A. Melzer, S. Cochran, M. P. MacDonald, and G. C. Spalding, Acoustic tractor beam, *Phys. Rev. Lett.* **112**, 174302 (2014).
- [17] Y. X. Li, C. Y. Qiu, S. J. Xu, M. Z. Ke, and Z. Y. Liu, Large-angle bending transport of microparticles by acoustic Half-Bessel beams, arXiv: 1411. 4776, 2014.
- [18] H. Estrada, F. J. Garcia de Abajo, P. Candelas, A. Uris, F. Belmar, and F. Meseguer,

Angle-dependent ultrasonic transmission through plates with subwavelength hole arrays, *Phys. Rev. Lett.* **102**, 144301 (2009).

[19] H. Estrada, P. Candelas, A. Uris, F. Belmar, F. J. Garcia de Abajo, and F. Meseguer, Influence of lattice symmetry on ultrasound transmission through plates with subwavelength aperture arrays, *Appl. Phys. Lett.* **95**, 051906 (2009).

[20] Z. J. He, S. S. Peng, R. Hao, C. Y. Qiu, M. Z. Ke, J. Mei, and Z. Y. Liu, Extraordinary acoustic reflection enhancement by acoustically transparent thin plates, *Appl. Phys. Lett.* **100**, 091904 (2012).

[21] Z. J. He, H. Jia, C. Y. Qiu, S. S. Peng, X. F. Mei, F. Y. Cai, P. Peng, M. Z. Ke, and Z. Y. Liu, Acoustic transmission enhancement through a periodically structured stiff plate without any opening, *Phys. Rev. Lett.* **105**, 074301 (2010).

[22] S. J. Xu, C. Y. Qiu, M. Z. Ke, and Z. Y. Liu, Tunable enhancement of the acoustic radiation pressure acting on a rigid wall via attaching a metamaterial slab, *Europhys. Lett.* **105**, 64004 (2014).

[23] C. Y. Qiu, S. J. Xu, M. Z. Ke, and Z. Y. Liu, Acoustically induced strong interaction between two periodically patterned elastic plates, *Phys. Rev. B* **90**, 094109 (2014).

[24] F. Y. Cai, L. Meng, C. X. Jiang, Y. Pan, and H. R. Zheng, Computation of the acoustic radiation force using the finite-difference time-domain method, *J. Acoust. Soc. Am.* **128**, 1617 (2010).

[25] F. G. Mitri, T. P. Lobo, and G. T. Silva, Axial acoustic radiation torque of a Bessel vortex beam on spherical shells, *Phys. Rev. E* **85**, 026602 (2012).

[26] F. M. Liu, F. Y. Cai, Y. Q. Ding, and Z. Y. Liu, Tunable transmission spectra of acoustic waves through double phononic crystal slabs, *Appl. Phys. Lett.* **92**, 103504 (2008).

[27] Z. J. He, C. Y. Qiu, L. Cheng, M. Xiao, K. Deng, and Z. Y. Liu, Negative-dynamic-mass response without localized resonance, *Europhys. Lett.* **91**, 54004 (2010).

[28] R. Hao, C. Y. Qiu, Y. Y. Hu, K. Tang, and Z. Y. Liu, Resonant transmission of acoustic waves through an elastic plate quasiperiodically corrugated on surfaces, *Phys. Lett. A* **375**, 4081 (2011).